Room-temperature synthesis of cyan $CsPb(Cl/Br)_3/SiO_2$ nanospheres with LiCl-H_2O solution

Peiyuan Cao (曹培源)[1], Bobo Yang (杨波波)[1,2,], Yanrong Cao (曹艳蓉)[3], Fei Zheng (郑 飞)[1], and Jun Zou (邹 军)[1,4,*]**

[1]*School of Science, Shanghai Institute of Technology, Shanghai 201418, China*
[2]*Institute of Future Lighting, Academy for Engineering and Technology, Fudan University, Shanghai 200433, China*
[3]*School of Materials Science and Engineering, Shanghai Institute of Technology, Shanghai 201418, China*
[4]*Institute of New Materials & Industrial Technology, Wenzhou University, Wenzhou 325024, China*
**Corresponding author: zoujun@sit.edu.cn; **corresponding author: boboyang@sit.edu.cn*
Received February 29, 2020; accepted April 16, 2020; posted online June 11, 2020

There are many strategies to maintain the excellent photoluminescence (PL) characteristics of perovskite quantum dots (QDs). Here, we proposed a facile and effective method to prepare cyan $CsPb(Cl/Br)_3/SiO_2$ nanospheres at room temperature. Cubic $CsPb(Cl/Br)_3$ was obtained by adding a LiCl-H_2O solution and anion exchange reaction. With (3-aminopropyl)triethoxysilane as an auxiliary agent, a QDs/SiO_2 composite was extracted from a sol-gel solution by precipitate-encapsulation method. The transmission electron microscopy images and Fourier transform infrared spectra indicated the QDs were indeed embedded in silica substances. Besides, humidity stability and thermal stability show the composite possesses a great application value. Finally, cyan $QDs@SiO_2$ powder has a high PL quantum yield of up to 84%; the stable cyan fluorescent powder does have great potential to play a key role in commercial full spectrum display.

Keywords: quantum dots; silicon dioxide; $CsPb(Cl/Br)_3$; lithium chloride; cyan.
doi: 10.3788/COL202018.071601.

Cesium lead halide (Cl, Br, I, or halide mixture) is considered to be a promising photoelectronic material, including employment in a light-emitting diode (LED), solar cell, laser, biomedical detection, and so on[1–5]. All of these superiorities contribute to their outstanding optical properties, such as facile controllable photoluminescence (PL) emission spectra, narrow full width at half-maximum (FWHM) of emission spectra and high PL quantum yield (PLQY)[1]. However, it is a major problem to maintain the optical properties of perovskite quantum dots (QDs) in air. Researchers have proposed a series of strategies to eliminate the defect of perovskite QDs. Actually, the QDs could still maintain outstanding optical properties after being treated by ion doping[6–14], surface passivation[15], and hybrid construction[16–33]. Therefore, balancing the stability and optical properties of perovskite QDs has become the focus of research.

Encapsulating QDs into other media has been considered an efficacious method to avoid their fluorescence degradation. Many facile methods were proposed to embed QDs into other materials to form cladding structures[18–29] and core-shell structures[16,17]. Actually, silica is an excellent choice to protect core materials because of its high stability and pellucidity. Besides, compounds of QDs/silica substrates can be simply fabricated into fluorescence powder and luminescence film. Whereafter, all kinds of QDs/silica structures were fabricated, including mesoporous silica[20,22], QDs/SiO_2 spheres[20,27,29], and QDs/SiO_2 Janus nanocrystals[33]. Silane reagents are commonly used to obtain silica, such as (3-aminopropyl)trimethoxysilane (APTMS)[6], (3-aminopropyl)triethoxysilane (APTES)[23,26,29], perhydropolysilazane (PHPS)[25], tetraethyl orthosilicate (TEOS)[34], and tetramethyl orthosilcate (TMOS)[28,35]. Especially, APTES is considered a typical silane reagent to form silica because of the extensive usage and budget price.

In this work, we synthesize $CsPbBr_3$ perovskite QDs at room temperature firstly[29,36]. Then, we use the anion exchange method to replace Br^- with Cl^- in a short time. At the same time of ion exchange reaction, APTES is gradually hydrolyzed into SiO_2. Finally, we can obtain $CsPb(Cl/Br)_3/SiO_2$ nanospheres with different emission wavelengths by coordinating the ion exchange time and chloride concentration[37–39]. The final product also has humidity stability and thermal stability. This efficient cyan $CsPb(Cl/Br)_3$ QD does make up for the lack of efficient cyan commercial phosphors.

As for the experimental process of synthesizing $CsPb(Cl/Br)_3@SiO_2$ spheres, first, 0.326 g (1 mmol) Cs_2CO_3 was dissolved in 5 mL *n*-octanoic acid (OTAc), keeping the solution stirring for 10 min to obtain the Cs precursor. Then, 0.367 g (1 mmol) $PbBr_2$ and 1.094 g (2 mmol) tetraoctylammonium bromide (TOAB) were added into 3 mL toluene, while the mixture was stirred for 15 min. By injecting 0.7 mL APTES into the $PbBr_2$-toluene and stirring for 20 s, 1.0 mL Cs precursor is rapidly added. After that, 180 μL LiCl-H_2O (2.01 g LiCl in 3 mL deionized water) was injected into the mixture. Whereafter, the precipitate was separated by centrifugation after 10 min of stirring. The deposit was dispersed in *n*-hexane, and the crude solution was recentrifuged. Finally, the as-prepared compound solid

needed to be dried for 48 h at 40°C to obtain QDs/SiO_2 powder.

The fabrication schematic of the $CsPb(Cl/Br)_3/SiO_2$ mixture solution is demonstrated in Fig. 1. In order to preserve and employ the luminous materials more conveniently, we extracted the QDs/SiO_2 compound from the sol-gel solution via centrifugation. Afterwards, we ground the drought-treated solid compound to luminescence powder. Actually, there are small facade changes when 180 μL of LiCl-H_2O solution was injected into $CsPbBr_3$/APTES mixture firstly. But, previously, the color of the mixture changes from yellow–green to cyan gradually. The process of color transformation was completed in about 10 min. This phenomenon indicates that the ion exchange reaction is fast and controllable. More importantly, the final samples emit intense cyan luminescence under ultraviolet (UV) light. Therefore, it is necessary to explore the reaction process and optical properties of the QDs/SiO_2 composite.

We performed a series of transmission electron microscopy (TEM) images of the final QDs/SiO_2 composite with different magnification. As shown in Fig. 2(a), many QDs/SiO_2 spheres were evenly distributed. Dispersed QDs/SiO_2 spheres also have similar dimensions. We calculated the size distribution of the $CsPb(Cl/Br)_3/SiO_2$ nanospheres [inset of Fig. 2(a)]. The average diameter of the nanospheres is 4.95 nm, while the maximum and minimum diameters are 9.38 nm and 2.15 nm, respectively. Besides, nanospheres in the 3.6 nm to 6.8 nm range accounted for 87% of the total statistics. We hypothesized that the silane reagent is responsible for the binding of particles. In this experiment, APTES is indeed involved in the combination of Pb^{2+}, Br^-, and Cs^+. In essence, APTES controls the growth of QDs. There are also many QDs attached to amorphous silica substrates [Fig. 2(b)] in our product. From Fig. 2(b), it can be observed that undispersed composite still maintains the shape of the spheres. To verify whether the mixed phases were formed by ion exchange, we measured the spacing of the lattice stripes and matched the results with the database. Three different values of 0.290 nm, 0.252 nm, and 0.278 nm correspond to the crystal faces of (2 0 0) ($CsPbBr_3$, JPCDS No. 54-0752), (2 1 0) ($CsPbCl_3$, JPCDS No. 75-0411), and (2 0 0) ($CsPbCl_3$, JPCDS No. 75-0411) in Fig. 2(c), respectively. Besides, selected area electron diffraction (SAED) of the nanoparticle indicates that final QDs product has high degrees of crystallinity [inset of Fig. 2(c)]. The above TEM images demonstrated the successful synthesis of $CsPb(Cl/Br)_3$@SiO_2 spheres.

We fabricated a series of samples by dropping different amounts of LiCl solution, while other experimental conditions remained exactly the same. After the calculation, 60 μL, 100 μL, 140 μL, and 180 μL of LiCl-H_2O correspond to 0.95 mmol, 1.58 mmol, 2.21 mmol, and 2.84 mmol of Cl^-, respectively. The specific ion content provides a basis for us to judge the degree of anion exchange. As depicted in Fig. 3(a), with the increase of the chloride dose, the emission wavelength decreased from 519 nm to 487 nm. Corresponding to Fig. 3(c), the color changed from green to cyan while the samples were exposed under UV irradiation ($\lambda = 365$ nm) [Fig. 3(c)]. Combining the PL spectra and the standard color

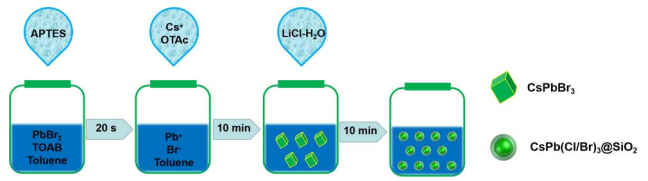

Fig. 1. Synthesizing schematic of the silica-coated $CsPb(Cl/Br)_3$ QDs.

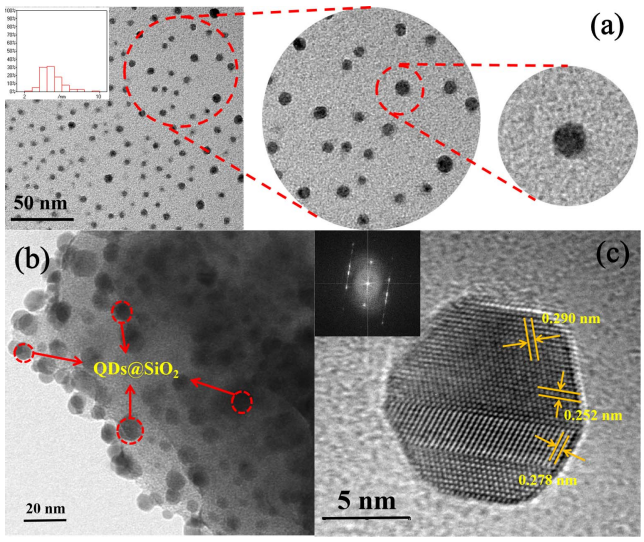

Fig. 2. TEM images of QDs@SiO_2 at different resolutions. Inset of (a) is the size distributions of the QDs@SiO_2 nanospheres. Inset of (c) is the corresponding SAED image.

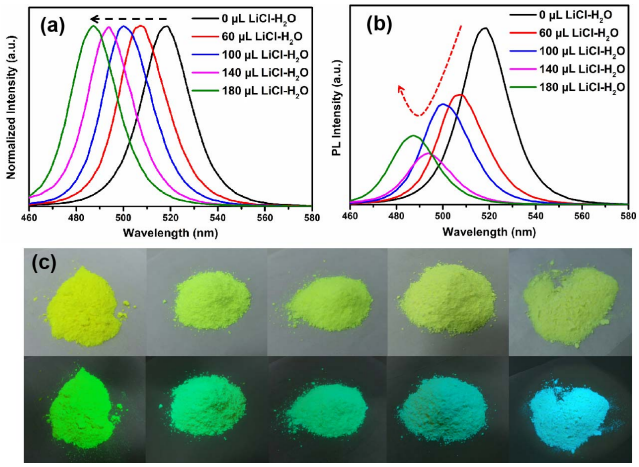

Fig. 3. (a) Normalized PL spectra and (b) original PL intensity spectra of the five samples when the amount of LiCl was 0/60/100/140/180 μL. (c) The pictures that recorded the compound powder (from left to right: 0 to 180 μL) exposed under the white fluorescent lamp (top row) and the UV light (bottom row), respectively.

spectrum, it can be speculated that the different concentrations of the Cl anion could prepare different colors of QDs product. In other words, we could adjust the amount of LiCl-H_2O to obtain tunable PL emission spectra. But, the PL intensity of the five samples has a tendency to go down first and then rise with the increase of Cl anion concentration [Fig. 3(b)]. It can be inferred that the Cl anion could gradually displace the Br anion *in situ* to form $CsPb(Cl/Br)_3$ within the initial period. As the amount of LiCl-H_2O rises from 140 μL to 180 μL, Cl ions dominate the perovskite halogen position that replaces Br ions. Besides, the weight of the sample ranges from 0.9 g to 1.0 g in our experiment. In the field of synthesizing $CsPbX_3$ QDs powder, a maximum yield of 1.0 g is indeed a high yield.

To verify our speculation, X-ray diffraction (XRD) equipment was utilized to characterize the composition of the QDs/SiO_2 composite [Fig. 4(a)]. The real peaks exhibit an obvious shift to higher angles compared with the $CsPbBr_3$ (JPCDS No. 54-0752) standard card, while the actual peaks display lower angles compared with $CsPbCl_3$ (JPCDS No. 75-0411). Combined with the overall peak variation trend, it can be learned that the composition of the material changes from the $CsPbBr_3$ phase [crystal structure of cubic $CsPbBr_3$ is shown in Fig. 4(b)] to the $CsPbCl_3$ phase. Combining PL spectra and XRD patterns, we can infer that $CsPb(Cl/Br)_3$ is generated. Besides, we found that the remaining peaks (12.6°, 20.1°, and rest of the small peaks) correspond to rhombohedral Cs_4PbBr_6 (JPCDS No. 73-2478). In our previous work, we proved that the generation of rhombohedral Cs_4PbBr_6 has no negative effect on optical properties of cubic $CsPbBr_3$[27]. Here, we can only make a preliminary guess at the cause of the increase in deionized water. The increase of water molecules breaks the ratio of Cs, Pb, and Br, resulting in the production of Cs_4PbBr_6.

Besides, we acquired the PL excitation (PLE) spectra [Fig. 5(a)] of the QDs/SiO_2. It can be found that the QDs behave in the broad excitation range from 350 nm to 460 nm. Besides, the similar trend of the curves indicates that the five samples have a similar essence. The PLE spectrum indicates that QDs/SiO_2 powder has uniform absorption ability from UV light to blue light. The immediate merit is that $CsPb(Cl/Br)_3/SiO_2$ could be employed in UV chips and blue chips indiscriminatingly. We also compared the Fourier transform infrared (FTIR) spectra of the $CsPb(Cl/Br)_3$@SiO_2 and SiO_2 [Fig. 5(b)].

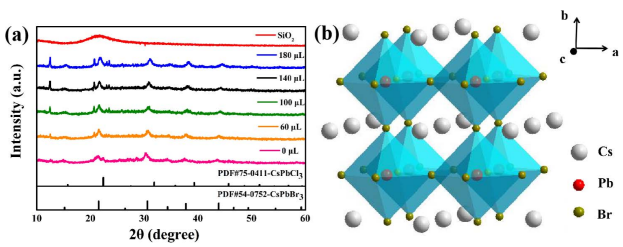

Fig. 4. (a) XRD patterns of the samples fabricated with different amounts of LiCl-H_2O. (b) Crystal structure of cubic $CsPbBr_3$.

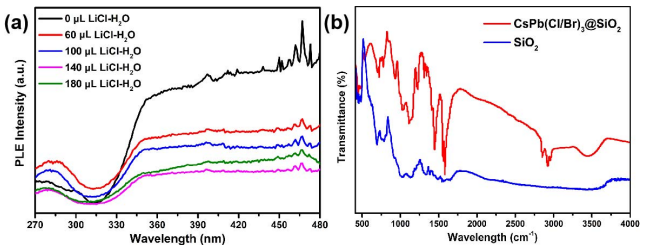

Fig. 5. (a) PLE spectra of the QD/SiO_2 composition and (b) FTIR spectra of the SiO_2 and $CsPb(Cl/Br)_3$@SiO_2 compounds.

The SiO_2 was prepared by natural hydrolysis of APTES at room temperature. The hydrolysis process occurs in a culture dish for more than 24 h without stirring. As shown in Fig. 5(b), the similarity of the two patterns indicates that the spontaneous hydrolysis of APTES has the same effect as that of accelerated hydrolysis. Besides, only several sharp peaks show the difference between two substances, including the ligands of some residual organics. Therefore, the message we can obtain from the figure is that the QDs we fabricated are indeed embedded in the silica substances.

The CIE color coordinates of $CsPb(Cl/Br)_3$ were also calculated. As shown in Fig. 6, the coordinates of the five samples are (0.106, 0.743), (0.063, 0.653), (0.053, 0.542), (0.060, 0.381), and (0.075, 0.266), respectively. The tendency of the QDs@SiO_2 changes from green to cyan indicated that the method we proposed does have the possibility to achieve blue emission pure $CsPbCl_3$@SiO_2 at room temperature. Actually, the $CsPbBr_3$@SiO_2 we synthesized before only has a PLQY of ~70%[27]. On that basis, we achieved a PLQY of 84% after adding 60 μL LiCl-H_2O solution. In fact, Cl can only partially replace Br on cubic $CsPbBr_3$ to form $CsPb(Cl/Br)_3$. There are still

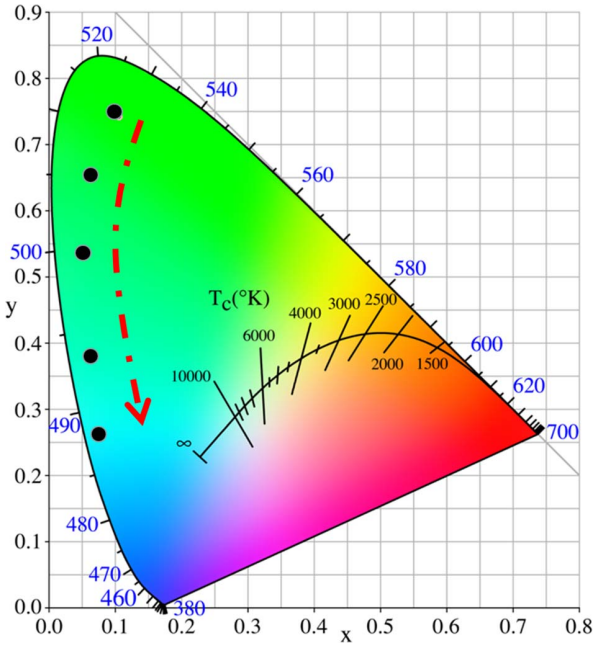

Fig. 6. Schematic of the CIE map (from top to bottom: 0/60/100/140/180 μL of LiCl-H_2O).

some free Cl^- and Li^+ in the sample. Underutilized Cl and Li produce a doping effect on $CsPbBr_3$. A series of tests were performed to verify the stability of QDs. The PL intensity of $CsPb(Cl/Br)_3@SiO_2$ powder can almost remain 100% after 30 min when treated in moist air (~85% humidity). Further, composites were rapidly heated to 105°C (~30 s) and then naturally cooled to room temperature (25°C); the PL intensity of $CsPb(Cl/Br)_3@SiO_2$ powder had little variation (~100%). The heating–cooling cycle test indicates that the luminescence characteristics of $CsPb(Cl/Br)_3@SiO_2$ are reversible. Finally, the cyan emission powder has a PLQY of 84% at the maximum, so this stable cyan $CsPb(Cl/Br)_3/SiO_2$ powder with high PLQY indeed has great potential to be employed in practice.

In summary, we successfully synthesized silica-wrapped $CsPb(Cl/Br)_3$ perovskite QDs at room temperature in open air. The QDs/SiO_2 composites were extracted from the sol-gel solution by using a precipitation-encapsulation method assisted with APTES. Cesium lead halide QDs with different wavelengths can be prepared by adjusting the concentration of the $LiCl\text{-}H_2O$. The $QDs@SiO_2$ composites with tunable wavelengths behave with improved stability and a high PLQY of 84%. Besides, humidity stability and thermal stability show that the $CsPb(Cl/Br)_3@SiO_2$ composite possesses great application value. The fabrication of cyan fluorescent powder indeed behaves with immense potential in a full spectrum display. The high yield of the powder is also performed with an industrial application prospect for large-scale preparation.

This work was supported by the Science and Technology Planning Project of Zhejiang Province (No. 2018C01046), Enterprise-Funded Latitudinal Research Projects of China (Nos. J2016-141, J2017-171, J2017-293, and J2017-243), Shanghai Sailing Program (No. 18YF1422500), and Research Start-Up Project of Shanghai Institute of Technology (No. YJ2018-9).

References

1. L. Protesescu, S. Yakunin, M. I. Bodnarchuk, F. Krieg, R. Caputo, C. H. Hendon, R. X. Yang, A. Walsh, and M. V. Kovalenko, Nano Lett. **15**, 3692 (2015).
2. Y. Wei, Z. Cheng, and J. Lin, Chem. Soc. Rev. **48**, 310 (2019).
3. F. Zheng, B. Yang, P. Cao, X. Qian, and J. Zou, J. Alloy. Compd. **818**, 153307 (2020).
4. S. Gu, P. Zhu, R. Lin, M. Tang, S. Zhu, and J. Zhu, Chin. Opt. Lett. **15**, 093501 (2017).
5. H. Fan, Y. Mu, C. Liu, Y. Zhu, G. Liu, S. Wang, Y. Li, and P. Du, Chin. Opt. Lett. **18**, 011403 (2020).
6. M. Yang, H. S. Peng, F. L. Zeng, F. Teng, Z. Qu, D. Yang, Y. Q. Wang, G. X. Chen, and D. W. Wang, J. Colloid Interface Sci. **509**, 32 (2018).
7. C. C. Lin, K. Y. Xu, and D. Wang, Sci. Rep. **7**, 45906 (2017).
8. M. He, Y. Cheng, L. Shen, C. Shen, H. Zhang, W. Xiang, and X. Liang, Appl. Surf. Sci. **448**, 400 (2018).
9. Z. Zhao, W. Xu, G. Pan, Y. Liu, M. Yang, S. Hua, X. Chen, H. Peng, and H. Song, Mater. Res. Bull. **112**, 142 (2019).
10. J. Ma, Q. Yao, J. A. Mcleod, L.-Y. Chang, C.-W. Pao, J. Chen, T.-K. Sham, and L. Liu, Nanoscale **11**, 6182 (2019).
11. D. Chen, G. Fang, and X. Chen, ACS Appl. Mater. Interfaces **9**, 40477 (2017).
12. M. He, Y. Cheng, L. Shen, H. Zhang, C. Shen, W. Xiang, and X. Liang, J. Am. Ceram. Soc. **102**, 1090 (2019).
13. G. Fang, D. Chen, S. Zhou, X. Chen, L. Lei, J. Zhang, and Z. Ji, J. Mater. Chem. C, **6**, 5908 (2018).
14. P. Wang, B. Dong, Z. Cui, R. Gao, and G. Su, RSC Adv. **8**, 1940 (2018).
15. G. H. Ahmed, J. K. El-Demellawi, J. Yin, J. Pan, D. B. Velusamy, M. N. Hedhili, E. Alarousu, O. M. Bakr, H. N. Alshareef, and O. F. Mohammed, ACS Energy Lett. **3**, 2301 (2018).
16. X. Chen, D. Chen, J. Li, G. Fang, H. Sheng, and J. Zhong, Dalton Trans. **47**, 5670 (2018).
17. X. Zhang, M. Lu, Y. Zhang, H. Wu, X. Shen, W. Zhang, W. Zheng, V. L. Colvin, and W. W. Yu, ACS Cent. Sci. **4**, 1352 (2018).
18. Y. H. Song, S.-Y. Park, J. S. Yoo, W. K. Park, H. S. Kim, S. H. Choi, S. B. Kwon, B. K. Kang, J. P. Kim, H. S. Jung, D. H. Yoon, W. S. Yang, and Y.-S. Seo, Chem. Eng. J. **352**, 957 (2018).
19. Y. Cai, L. Wang, T. Zhou, P. Zheng, Y. Li, and R. J. Xie, Nanoscale, **10**, 21441 (2018).
20. X. Hu, P. Zrazhevskiy, and X. Gao, Ann. Biomed. Eng. **37**, 1960 (2009).
21. J. Ren, T. Ren, X. Zhou, X. Dong, A. V. EShorokhov, M. B. Semenov, V. D. Krevchikc, and Y. Wang, Chem. Eng. J. **358**, 30 (2018).
22. D. N. Dirin, L. Protesescu, D. Trummer, I. V. Kochetygov, S. Yakunin, F. Krumeich, N. P. Stadie, and M. V. Kovalenko, Nano Lett. **16**, 5866 (2016).
23. C. Sun, Y. Zhang, C. Ruan, C. Yin, X. Wang, Y. Wang, and W. W. Yu, Adv. Mater. **28**, 10088 (2016).
24. W. Chen, T. Shi, J. Du, Z. Zang, Z. Yao, M. Li, K. Sun, W. Hu, Y. Leng, and X. Tang, ACS Appl. Mater. Interfaces **10**, 43978 (2018).
25. D. H. Park, J. S. Han, W. Kim, and H. S. Jang, Dyes Pigm. **149**, 246 (2018).
26. F. L. Zeng, M. Yang, J. L. Qin, F. Teng, Y. Q. Wang, G. X. Chen, D. W. Wang, and H. S. Peng, ACS Appl. Mater. Interfaces **10**, 42837 (2018).
27. Q. Xiang, B. Zhou, K. Cao, Y. Wen, Y. Li, Z. Wang, C. Jiang, B. Shan, and R. Chen, Chem. Mater. **30**, 8486 (2018).
28. S. Huang, Z. Li, L. Kong, N. Zhu, A. Shan, and L. Li, J. Am. Chem. Soc. **138**, 5749 (2016).
29. P. Cao, B. Yang, F. Zheng, L. Wang, and J. Zou, Ceram. Int. **46**, 3882 (2020).
30. F. Zhang, Z. Shi, S. Li, Z. Ma, Y. Li, L. Wang, D. Wu, Y. Tian, G. Du, X. Li, and C. Shan, ACS Appl. Mater. Interfaces **11**, 28013 (2019).
31. Z. Shi, S. Li, Y. Li, H. Ji, X. Li, D. Wu, T. Xu, Y. Chen, Y. Tian, Y. Zhang, C. Shan, and G. Du, ACS Nano **12**, 1462 (2018).
32. F. Zhang, Z. Shi, Z. Ma, Y. Li, S. Li, D. Wu, T. Xu, X. Li, C. Shan, and G. Du, Nanoscale, **10**, 20131 (2018).
33. Z. Shi, Y. Li, Y. Zhang, Y. Chen, X. Li, D. Wu, T. Xu, C. Shan, and G. Du, Nano Lett. **17**, 313 (2017).
34. N. Ding, D. Zhou, X. Sun, W. Xu, H. Xu, G. Pan, D. Li, S. Zhang, B. Dong, and H. Song, Nanotechnology **29**, 345703 (2018).
35. H. Hu, L. Wu, Y. Tan, Q. Zhong, M. Chen, Y. Qiu, D. Yang, B. Sun, Q. Zhang, and Y. Yin, J. Am. Chem. Soc. **140**, 406 (2018).
36. J. Song, J. Li, L. Xu, J. Li, F. Zhang, B. Han, Q. Shan, and H. Zheng, Adv. Mater. **30**, 1800764 (2018).
37. X. Chen, D. Chen, J. Li, G. Fang, H. Sheng, and J. Zhong, Dalton Trans. **47**, 5670 (2018).
38. J. Zhu, Q. Di, X. Zhao, X. Wu, X. Fan, Q. Li, W. Song, and Z. Quan, Inorg. Chem. **57**, 6206 (2018).
39. P. Somg, B. Qiao, D. Somg, Z. Liang, D. Gao, J. Cao, Z. Shen, Z. Xu, and S. Zhao, J. Alloys Compd. **767**, 98 (2018).